Electronic field emission models beyond the Fowler-Nordheim one

Bruno Lepetit

Electronic field emission models beyond the Fowler-Nordheim one

Bruno Lepetit*

Laboratoire Collisions Agrégats Réactivité,

UMR5589, Université de Toulouse, CNRS,

Bât. 3R1b4 - 118 route de Narbonne 31062 Toulouse Cedex 09, France

(Dated: November 3, 2017)

Abstract

We propose several quantum mechanical models to describe electronic field emission from first principles. These models allow to correlate quantitatively the electronic emission current to the electrode surface details at the atomic scale. They all rely on electronic potential energie surfaces obtained from three dimensional density functional theory calculations. They differ by the various quantum mechanical methods (exact or perturbative, time dependent or time independent) which are used to describe tunneling through the electronic potential energy barrier. Comparison of these models between them and with the standard Fowler-Nordheim one in the context of one dimensional tunneling allows to assess the impact on the accuracy of the computed current of the approximations made in each model. Among these methods, the time dependent perturbative one provides a well balanced trade-off between accuracy and computational cost.

I. INTRODUCTION

Electronic emission[1,2] induced by static electric field can cause vacuum electrical breakdown. This poses challenges to the design of vacuum insulation structures in high voltage systems, especially nowadays for the nuclear fusion industry. Indeed, one of the heating strategies of magnetically confined plasma in tokamaks uses high energy hydrogen or deuterium atoms accelerated by the electric field of a high voltage system, the performance of which is severely limited by damaging electron currents resulting from field emission[3–6]. These currents can be reduced by raising the pressure in the vacuum system, typically from ultrahigh vacuum to pressures of the order of $10^{-4} - 10^{-2}$ Pa[7–13]. This gas effect, known for quite some time, has been investigated recently in details for tungsten carbide and tungsten cathodes[14–18].

It is known that such current variations correlated to changes in ambient pressure are related to modifications in the cathode surface state at the atomic scale, but there is no consensus on the nature of these changes. Some believe that they result from adsorption of ambient gases or other contaminants[12,19]. In a recent experimental study, the main contaminant was found to be carbon[17]. Others attribute the gas effect to the transformation of sharp emitting tips into blunt ones by sputtering from ion bombardment localized near emitting protrusions[8–10]. Accurate emission models from first principles are required to understand better the correlations between surface states at the atomic scale and emission properties. Unfortunately, most of them are currently too crude to provide such detailled information.

Indeed, our understanding of electronic emission still relies mainly on the historical Fowler-Nordheim model[1,20], corrected in ref. 21, extented to thermo-ionic emission by Murphy and Good in ref. 2, to curved emitters in ref. 22. A generalization using the local density of states at the surface has been proposed in ref. 23. Convenient simplifications of the analytical functions involved in this model have been given in ref. 24. A universal formulation of the model has been proposed in ref. 25. It has been used widely and successfully over the years as a fitting model of experimental data, recent examples of applications are given in the references of ref. 26,27. This model, referred to as the SFN (Standard Fowler Nordheim) model in the following, describes electron emission as a one dimensional tunneling process through a simple analytical electronic potential energy barrier. Tunneling probability is

obtained from an approximate semi-classical JWKB (Jeffreys–Wentzel–Kramers–Brillouin) approximation. In fact, this model relies on a crude description of the emitting electrode by a single parameter, the work function. It is more a semi-empirical model than an *ab initio* one and it can barely correlate emission to the surface structure details such as the presence of defects or individual adsorbed atoms or molecules.

The design of more quantitative models has therefore been the goal of more recent investigations, in particular in the context of the development of carbon based nanomaterials (for reviews, see ref. 28,29). The first step common to these methods is a Density Functional Theory (DFT) calculation of the Hartree and exchange-correlation potentials which drive electron emission. The second step is the modelling of the emitted electron dynamics. One class of such models involves improvements of the Fowler-Nordheim models and their adaptation to the context of DFT potentials[29]. Although the equation used to compute the emitted current is one dimensional, the potential energy surface it relies on can be extracted from three dimensional data (see for instance ref. 30), also facetization of the emitting structure allows to take into account complex structures[31]. A second class of methods uses Schrödinger-like equations to describe the electron dynamics, and solve them either by time dependent or by time independent quantum mechanical methods. Concerning time independent methods, we find wavefunction propagation methods, mainly in the context of one dimensional problems[32–35] but close-coupling type extensions to full dimensionality have also been attempted[36,37]. The cylindrical symetry of carbon nanotubes has been taken advantage of in ref. 38. Alternatively, non-equilibrium time independent Green 's function[39] and Fisher-Lee 's transmission formulation[40] have also been used. Time dependent methods involve propagation of a wavepacket describing the emitted electrons[41]. The emitted current is obtained by a fit of the decay (linear at short times) of the residual charge in the material. This model has been used in studies of emission from double-wall carbon nanotubes[42] and metal nanowires[43]. However, these methods have found limited applications because of implementation difficulties. For instance, concerning time dependent methods, the decrease of the charge is very slow at the atomic scale (for usual external field values) and large integration times have to be reached for significant decrease to be observed. The external field, which is typically less than 5 GV/m, is indeed smaller than the intrinsic electric field experienced by the electrons at the material/vacuum interface, typically more than 10 GV/m. The external field acts as a weak perturbation on the electrons of the electrode.

This suggests that perturbative methods may be well adapted to model electronic emission in standard engineering conditions. We speculate that the simplifications resulting from the use of such approximate formalisms may reduce the formal and computational difficulties of the numerical implementations. Validating this hypothesis is the main goal of the present paper.

We present in section II the different models developed for the present study. We first introduce in subsection II A a general framework common to all the methods presented here. We recast in subsection II B the SFN model in a form suitable for subsequent extensions. Then, we substitute a numerical DFT electronic potential energy to the crude analytical one of the SFN model. Tunneling through this DFT electronic potential energy barrier is subsequently computed. This can be achieved with the approximate semi-classical JWKB method of the original SFN model, this corresponds to the Numerical Fowler Nordheim (NFN) model in the following. Alternatively, tunneling through the same DFT barrier can be computed with an Exact Quantum Mechanical (EQM) numerical method. These NFN and EQM models are described in subsection II C. They both suffer however from severe limitations. Because it relies on the JWKB method, the NFN model, similarly to the SFN method, can not be applied to realistic three dimensional (3D) problems. The EQM does not suffer from this formal limitation, but applications to 3D problems encounter implementation difficulties, similar to those exposed in the preceeding paragraph. Our proposal to use the quantum mechanical perturbation theory to overcome these difficulties is implemented in Time-Independent and Time-Dependent Pertubative models (named TIP and TDP models, respectively) presented in subsections II D and II E.

We then apply these different methods in sections III and IV to predict emission from a tungsten cathod. The DFT model of the cathode is described in subsection III A and the potentials and states drawn from it in subsection III B. The computed currents are presented and discussed in section IV. We validate our use of the perturbation theory by comparing TIP and TDP emitted currents with the SFN, NFN and EQM ones. We trace back the relative contributions to the error in the current to the approximations inherent to each of these models. Conclusion follows (section V).

II. COMPUTATIONAL METHODS

A. General framework

In the following, bold-face symbols refer to vectors, the corresponding standard symbols refer to their norms. We consider the electrons of a metallic slab infinite in the x and y directions and of finite thickness L in z, subjected to an external field $\mathbf{F}$ parallel to z. An electronic current then flows from the metal into the vacuum and we investigate numerical methods which have sufficient accuracy to predict this emitted current from the definition of the surface structure at the atomic level, including defects and adsorbates, and which at the same time can be related to the widespread semi-empirical SFN model. Therefore, we describe in this section a hierarchy of improvements to the SFN picture leading to *ab-initio* models where the emitted current is related more closely to the details of the emitting metal. We assume that the emitting surface is at 0 K temperature. We assume that the electrons occupy orbitals $\Psi_m(\mathbf{r}, \mathbf{F} = 0)$ defined by :

$$(T + U(\mathbf{r}, \mathbf{F} = \mathbf{0}))\, \Psi^b_m(\mathbf{r}, \mathbf{F} = 0) = \epsilon_m\, \Psi^b_m(\mathbf{r}, \mathbf{F} = 0) \tag{1}$$

T is the electronic kinetic energy operator and $U(\mathbf{r}, \mathbf{F} = \mathbf{0})$ is the total potential energy experienced by an electron of the material located at $\mathbf{r}$ in the absence of external field. The $\Psi^b_m(\mathbf{r}, \mathbf{F} = 0)$ orbitals are Bloch functions (p. 179 in ref. 44). They are labelled by the composite state index m which provides their electron momentum in the first Brillouin zone (p. 37 in ref. 44) and the band to which they belong. The solutions of eq. 1 form a continuum of states which can extend to infinity in the $x\,y$ plane. In practice, periodic conditions are applied at the boundary of a portion of the slab Ω consiting of N_k unit cells and usually called a supercell (see for instance ref. 45, p. 35). Applying such boundary conditions is equivalent to discretizing the first Brillouin zone with N_k k-points. The orbitals are normalized such that they correspond to one electron charge over Ω.

When the external field is applied, the electrons are no more confined to Ω, they can leak into vacuum. We call the leakage rate of each orbital, I_m, a "state current". Notice that the notion of "state current" introduced here is less common in the field emission community than the one of "state current density" one introduced in ref. 46. It should be pointed out that in the present context of a possibly non uniform emitting surface, the state current density is local quantity depending on the location on the surface, whereas the state current

is a global quantity. Both quantities contain the same information in the context of a uniform surface considered in ref 46.

It should be noticed however that neither state current nor state current density are accessible to experiments. A summation over the states is necessary to obtain a measurable quantity. The total current emitted by Ω is :

$$I_\Omega = 2\sum_m I_m \tag{2}$$

assuming double occupancy of each orbital because of the Pauli exclusion principle. An averaged emitted current density over Ω can be obtained simply from :

$$J = \frac{I_\Omega}{N_k A_{uc}} \tag{3}$$

where A_{uc} is the area of the intersection of the unit cell and the $x\,y$ plane. This current density can be measured in the ideal context of a perfectly clean surface. We now describe different levels of approximations to obtain this averaged currrent density.

B. The standard Fowler-Nordheim model

We now derive the SFN model (ref. 1,2, see also ref. 26,27) by performing drastic simplifying assumptions to the general framework presented in subsection II A. First, we assume that the slab is invariant in the xy plane so that the motion of the electrons in the plane can be described by plane waves. The orbitals (eq. 1) are now labelled by the electron momentum parallel to the plane $\mathbf{k_{xy}}$ and a discrete index j associated to the bound orbitals $\psi_j(z)$:

$$\Psi^b_{\mathbf{k_{xy}},j}(\mathbf{r}, \mathbf{F}=0) = \frac{1}{\sqrt{N_k A_{uc}}} e^{i\mathbf{k_{xy}}\mathbf{r}} \psi^b_j(z) \tag{4}$$

The current associated to the state $\Psi^b_{\mathbf{k_{xy}},j}(\mathbf{r}, \mathbf{F}=0)$ depends only on the kinetic energy along the z direction : $\epsilon_z = \frac{\hbar^2 k_z^2}{2m}$ (k_z : corresponding wavevector, $\hbar$: Planck constant, m : electron mass) and is referred to as $I(\epsilon_z)$. Computation of the total current from eq. 2 now requires a straightforward integration over $\mathbf{k_{xy}}$ as well as a summation on j which becomes an integral over k_z if we substitute plane waves periodic over L to the bound states $\psi^b_j(z)$. The result is :

$$I_\Omega = 2\int_{\epsilon_z<\epsilon_F} dk_z \frac{L}{2\pi} n_\Omega(\epsilon_z) I(\epsilon_z) \tag{5}$$

where ϵ_F is the Fermi energy. $n_\Omega(\epsilon_z)$ is the number of states of a two dimensional free electron gaz of area $N_k A_{uc}$ at energy $\epsilon_F - \epsilon_z$: $n_\Omega(\epsilon_z) = \frac{m(\epsilon_F - \epsilon_z)}{2\pi\hbar^2} N_k A_{uc}$

The second ingredient of the model is to write the state current as :

$$I(\epsilon_z) = e\rho \frac{\hbar k_z}{m} D(\epsilon_z) \tag{6}$$

where e is the elementary positive charge. ρ is the electronic density, but we substitute to its true value, $\rho = |\psi_j^b(z)|^2$, the one for a one dimensional normalized plane wave : $\rho = \frac{1}{L}$. $D(\epsilon_z)$ is the transmission through a potential energy barrier, responsible for the electron leakage.

Insertion of eq. 6 into eq. 5 provides :

$$I_\Omega = \frac{e}{\pi\hbar} \int_{\epsilon_z < \epsilon_F} d\epsilon_z n_\Omega(\epsilon_z) D(\epsilon_z) \tag{7}$$

This integral can be calculated approximately by performing a Taylor expansion of the transmission near the Fermi energy. Using eq. 3 and 7 and following ref. 46, we obtain for the current density :

$$J = s_S d_F^2 D(\epsilon_F) \tag{8}$$

where s_S is the so-called Sommerfeld's electron supply constant[46] : $s_S = \frac{em}{2\pi^2\hbar^3}$, and $d_F^{-1} = \frac{d\, ln D(\epsilon_z)}{d\epsilon_z}|_{\epsilon_z = \epsilon_F}$. In terms of the state current at Fermi level, we obtain using eq. 6 :

$$J = s_S d_F^2 \frac{m}{e\rho\hbar k_F} I(\epsilon_F) \tag{9}$$

where $k_F = k_z$ at the Fermi energy. The original Fowler-Nordheim theory as well as the Murphy-Good improvement were obtained for a particular potential energy which consists in the simple superposition of a charge-image interaction and of a linear external variation in electrostatic potential energy :

$$U(z) = -\frac{e^2}{16\pi\varepsilon_0(z - z_s)} - eF(z - z_s) + U_{vac} \tag{10}$$

(z_s : surface position, ε_0 : electric constant, U_{vac} : local vacuum level, measured relative to the base of the conduction band). In this case, the tunneling probability can be obtained analytically from the approximate semiclassical JWKB method (p. 158 in ref. 47) :

$$D(\epsilon_z) = \exp\left(-\frac{4}{3e} \left(\frac{2m}{\hbar^2} \right)^{\frac{1}{2}} \frac{(U_{vac} - \epsilon_z)^{\frac{3}{2}} v(y)}{F} \right) \tag{11}$$

$v(y)$ is a function of the variable $y = \frac{\left(\frac{e^3F}{4\pi\varepsilon_0}\right)^{\frac{1}{2}}}{U_{vac}-\epsilon_z}$. It can be expressed in terms of complete elliptic integrals and it can also be approximated by simpler expressions[24]. Inserting eq. 11 into eq. 8 provides the usual result :

$$J = \frac{e^3F^2}{16\pi^2\hbar\varphi(t(y_F))^2}\exp\left(-\frac{4}{3e}\left(\frac{2m}{\hbar^2}\right)^{\frac{1}{2}}\frac{\varphi^{\frac{3}{2}}v(y_F)}{F}\right) \tag{12}$$

where $\varphi = U_{vac} - \epsilon_F$ is the work function, y_F the value of y for $\epsilon_z = \epsilon_F$ and $t(y) = v(y) - \frac{2}{3}y\frac{dv(y)}{dy}$.

In the following, we will use the expression given by eq. 9 to improve the SFN model with predictions for $I(\epsilon_F)$ more accurate than the ones obtained within the SFN model for an analytical potential energy with the JWKB method.

C. Improved Fowler-Nordheim models

Refined numerical potential energies obtained from DFT calculations can be substituted to the simple analytical expression of eq. 10. We provide details on the numerical method we use to obtain such potential energies in subsection III A. Since such computations provide 3D potential energy surfaces, a procedure has to be implemented to extract a one dimensional potential from the 3D one for the purpose of the comparison with the SFN model which is the scope of the present study. Such a procedure is described in subsection III B. Obviously, the emitted current density for such numerical potential energies cannot be obtained any more from an analytical expression, but several numerical methods can be used to compute the transmission probability and the emitted current.

The simplest improvement is to continue to apply the semiclassical JWKB approximation, but now integrating numerically rather than analytically the local wavevector in the tunneling region. Eq. 9 can still be applied with this new transmission $D(\epsilon_F)$. We call this method the Numerical Fowler-Nordheim (NFN) method.

Alternatively, one can solve numerically the Schrödinger equation describing the electron tunneling process without semiclassical approximation. This was done in ref. 48 using the transfer matrix technique. Here, we use a wavefunction propagation method. The purely outgoing solution at large distance describing electrons emitted in the vacuum at energy ϵ is known to be proportional to the complex combination of Airy functions

$Bi\left(-(\epsilon - U(z))\,\frac{(2m)^{\frac{1}{3}}}{(\hbar eF)^{\frac{2}{3}}}\right) + i\,Ai\left(-(\epsilon - U(z))\,\frac{(2m)^{\frac{1}{3}}}{(\hbar eF)^{\frac{2}{3}}}\right)$ since the potential is linear in this region (ref. 47, p. 73). A solution satisfying this boundary condition can be obtained by numerical spatial integration from this vacuum region to the metal region. Once the wave-function is known in both regions of space, a new transmission probability $D(\epsilon_F)$ can be extracted straightforwardly, and then again, emitted current can be obtained using eq. 9. We refer to this method as the Exact Quantum Mechanical (EQM) method.

D. Time independent perturbative models

In the present context of field emission, the external field is orders of magnitude smaller than the intrisic electrostatic field (i.e. the one experienced by the electrons of the material without external field), in particular in the vicinity of the material/vacuum interface[18]. It is therefore reasonable to study the effect of the external field on electronic emission using perturbation theory. The formalism is presented for a full 3D potential energy surface but it is also implemented here to one dimension cases to allow for comparison with the usual Fowler-Nordheim and Murphy-Good models. This formalism provides an electronic current associated to each quantum state of the emitting material (see eq. 6). The state current at the Fermi energy $I(\epsilon_F)$ is inserted in eq. 9 to obtain the global emitted current density J.

The total potential energy is split as follows : $U(\mathbf{r},\mathbf{F}) = U(\mathbf{r},\mathbf{F}=\mathbf{0}) + \Delta U(\mathbf{r},\mathbf{F})$. $\Delta U(\mathbf{r},\mathbf{F})$ is the perturbation associated with the external field : it vanishes inside the metal and its gradient assumes the linear form $-e\mathbf{F}$ far away from the metal.

We define continuum states for emitted electrons labelled by their energy ϵ and state index n :

$$(T + \Delta U(\mathbf{r},\mathbf{F}) + U_{vac})\,\Psi^c_{\epsilon,n}(\mathbf{r},\mathbf{F}) = \epsilon\,\Psi^c_{\epsilon,n}(\mathbf{r},\mathbf{F}) \tag{13}$$

The state index n now describes the different possible values of the electronic momentum of the continuum state far from the surface. We enforce the energy normalization condition $< \Psi^c_{\epsilon,n}(\mathbf{r},\mathbf{F})|\Psi^c_{\epsilon',n'}(\mathbf{r},\mathbf{F}) >= \delta(\epsilon-\epsilon')\,\delta_{nn'}$. The standard Fermi golden rule (ref. 47, p. 147) then provides the emission rate induced by the external field $\mathbf{F}$ from the initial bound state ϵ_b, m as 3D integrals which, multiplied by the electron charge, provides the currents :

$$I_m = \frac{2\pi e}{\hbar}\sum_n |< \Psi^b_m(\mathbf{r},\mathbf{F}=0)|\Delta U(\mathbf{r},\mathbf{F})|\Psi^c_{\epsilon_b,n}(\mathbf{r},\mathbf{F}) >|^2 \tag{14}$$

This is the expression for the state current of eq. 6 in the Time Independent Perturbation (TIP) model. It can also be viewed as the result of a generalized Born expansion (ref. 49, chapter 15.3, p. 832-841) of the matrix element of the evolution operator connecting initial and final states which are eigenvectors in different spaces. The energy normalized continuum state $\Psi^c_{\epsilon,n}(\mathbf{r},\mathbf{F})$ which represents electrons emitted to infinity may be unconvenient to compute in the 3D case. However, for one dimensional tunneling which is the context of the SFN model, eq. 13 has a simple analytical solution. Indeed, the solution which vanishes inside the metal can be obtained analytically for a linear approximation to $\Delta U(z,F)$ (see subsection III B below) : $\Psi^c_{\epsilon_b}(z,F) = NAi\left(-\left(\frac{2mFe}{\hbar^2}\right)^{\frac{1}{3}}(z - z_T(\epsilon_b))\right)$ ($z_T(\epsilon_b)$: turning point at energy ϵ_b). The normalization constant N is obtained by enforcing the energy normalization condition on the asymptotic form of this solution, this provides : $N = \left(\frac{4m^2}{\hbar^4 eF}\right)^{\frac{1}{6}}$. Once the bound states are obtained from eq. 1, for instance by expansion on a basis set, the state currents are computed from eq. 14 by numerical quadratures. The current for $\epsilon_b \approx \epsilon_F$ is injected in eq. 9 to give the TIP current density emitted by the material.

E. Time dependent perturbative models

There exists a Time-Dependent version of the Perturbation (TDP) method which avoids the difficult computation of the 3D continuum states. This time-dependent Fermi Golden rule method has been used extensively, for instance, in the field of molecular photodissociation[50]. The present work is an extension of the use of this method to electronic emission. We first consider a new state, defined as the action of the perturbation on the initial bound state $|\Phi_m(\mathbf{r},\mathbf{F}) >= \Delta U(\mathbf{r},\mathbf{F})|\Psi^b_m(\mathbf{r},\mathbf{F}=0) >$. The time evolution of this state induced by the external field is obtained by applying the evolution operator and the corresponding correlation function can be computed as : $C_{\epsilon_b,m}(t) =< \Phi_m|e^{-i\frac{T+\Delta U(\mathbf{r},\mathbf{F})+U_{vac}}{\hbar}t}|\Phi_m >$. The correlation function is much easier to compute in the present perturbative framework than in the non perturbative wave packet propagation formalism[41] because it decays here very quickly to 0. Indeed, the wavepacket $|\Phi_m >$ is expelled quickly from the vicinity of the emitting material where it is initially located by the strongly repulsive $\Delta U(\mathbf{r},\mathbf{F})$ potential energy. It can then be shown[50] that the current of eq. 14 is simply the Fourier transform of this correlation function :

$$I_m = \frac{e}{\hbar^2}\int_{-\infty}^{+\infty} dt e^{i\frac{\epsilon_b t}{\hbar}} C_m(t) \tag{15}$$

We make two uses of this current. One is to inject its value for $\epsilon_m \approx \epsilon_F$ in eq. 9, this provides the TDP current density emitted by the material. This a simple hybrid version of the TDP method mixing perturbation theory and the Fowler-Nordheim model of the material. Alternatively, a numerically more challenging three dimensional version of the method can also be implemented. Indeed, eq. 15 can also be used with full three dimensional orbitals $|\Psi^b_m(\mathbf{r}, \mathbf{F} = 0) >$ to compute individual state currents and the total current can be obtained by direct summation of these contributions (eq. 2). We refer to this method as the TDP-3D one.

III. NUMERICAL IMPLEMENTATION

A. Potential energies and states

We now illustrate the use of the different methods described above on the electronic emission from flat (100) surfaces of bcc tungsten. This commonly used material for electrodes has already been the subject of numerous studies using DFT (see our recent work, ref. 16–18 and references therein). Many properties of the material have been studied in depth : cohesive energy, lattice constant a and elastic parameters, relaxation, reconstruction parameters and surface formation energies, work functions... The effect on electronic emission of carbon adsorption[16] and of surface nanoscale structures[18] was also modeled and compared to experimental results[17].

The structure considered in the present study is a slab of 17 atomic planes limited on both sides by a (100) surface chosen to be the xy plane. Its thickness is $L = 8\,a$. The slab is embedded in a static electric field parallel to z, one of its sides plays the role of the cathode and emits electrons while the other is the anode[18]. The slab is thick enough for the interaction between both sides to be negligible, emission from its cathode side is the same as from a macroscopic size electrode. The unit cell contains one atom per layer, shifted between neighboring planes by $a/2$ in both x and y directions to generate by periodicity the bcc structure. Using results from our previous studies[16], the lattice parameter is chosen as $a = 3.179$ Å and the work function is $\varphi = 4.2$ eV.

The ab initio total-energy and molecular dynamics program VASP (Vienna ab initio simulation program) developed at the Institut für Materialphysik of the Universität Wien

has been used for all DFT calculations[51–54]. We use this program in a way very similar to the one already described in refs. 16,18. The electron-ion interaction for tungsten is described by the projector augmented wave potential (PAW)[55,56]. The exchange-correlation energy is calculated within the generalized gradient approximation (GGA) using the revised form of the Perdew, Burke, and Ernzerhof functional (PBE)[57–59]. We consider six $5d6s$ valence electrons for each tungsten atom and we use the convergence parameters resulting from a previous study[16]. Fractional occupancies are calculated using a second-order Methfessel-Paxton smearing function[60] with a width of 0.2 eV. All plane waves of the basis set are expanded up to a kinetic energy cutoff of 223 eV and we use a $(8 \times 8 \times 1)$ k-point grid and we checked convergence by comparison with $(7 \times 11 \times 1)$ and $(5 \times 15 \times 1)$ grids. The slab is part of a supercell $20\,a$ thick. In presence of the external field, an artificial dipole must be added in the vacuum region to allow for periodicity of the electrostatic potential between the upper and lower rim of the supercell. This correction also cancels the long range dipolar interactions between the periodic replicates of the structure in the z direction.

B. DFT results post-processing

VASP provides 3-dimensional Hartree (electrostatic) $U_H(\mathbf{r}, \mathbf{F})$ and total (Hartree+exchange-correlation) potentials $U(\mathbf{r}, \mathbf{F}) = U_H(\mathbf{r}, \mathbf{F}) + U_{XC}(\mathbf{r}, \mathbf{F})$ for a given external field $\mathbf{F}$. These potential energies present deep minima close to the nuclei and are relatively flat between them. The total potential energies along the z line $x = a/2$, $y = 0$ are shown on fig. 1 for $F = 0$ and $F = 0.5$ GV/m. These potentials do not depend significantly on the external field amplitude inside the slab. There, they are not far from being constant, which is expected as the chosen line avoids all nuclei, and present only weak oscillations around the average value -10 eV. Such a behavior is qualitatively consistent with the free electron Fowler-Nordheim and Murphy-Good picture for metals. This justifies why, in the following, we use the z line $x = a/2$, $y = 0$ to define the one-dimensional potential-energy barriers used in conventional field emission theory.

VASP also provides the expansions of the Kohn-Sham orbitals on a plane-wave basis for the different wavevector values and bands. We obtained the values of these orbitals on a 3D spatial grid using our implementation based on fast Fourier transforms of the post-processing Wavetrans[61]. We use these Kohn-Sham orbitals as the orbitals $\Psi_m^b(\mathbf{r}, \mathbf{F} = 0)$ (eq.

1) in our formalism (subsection II A). One may question the validity of such a choice, as it is well known that Kohn-Sham orbitals are in general computation intermediates without specific physical meaning. It is known, however, that the total density which is obtained by summation of the orbital amplitudes squared is physically correct. By similarity, we assume here that the total current which is obtained by summation of the state currents (eq. 2) is also physically meaningful.

The perturbative potential $\Delta U(\mathbf{r}, \mathbf{F})$ which induces emission should in principle be obtained from the difference $U(\mathbf{r}, \mathbf{F}) - U(\mathbf{r}, \mathbf{F} = \mathbf{0})$ of two different VASP computations. However, we experienced convergence problems with VASP for fields of the order of 1 GV/m or larger. Fig. 1 (right scale) compares $\Delta U(\mathbf{r}, \mathbf{F} = 0.5 \text{ GV/m})$ obtained from two VASP calculations with the simple linear approximation $-eF(z - z_s)$, where z_s is the extreme atomic layer position. This simple linear approximation follows closely the numerical result $\Delta U(\mathbf{r}, \mathbf{F} = 0.5 \text{ GV/m})$, but with a shift in z which is of the order of 2 Å both on the anode and cathode sides. This shift is the result of the displacement of the induced charge away from the surface[18], it is equivalent to the repulsion distance used in the charged surface theory in the field ion emission context[62,63]. In the following, we assume that the simple linear approximation : $\Delta U(z, F) = -eF(z - z_s)$, is valid even for the strongest external fields.

The bound states $\Psi^b_m(\mathbf{r}, \mathbf{F} = 0)$ which emit electrons are obtained as the eigenstates of the Hamiltonian associated to the one-dimensional total potential energy for $F = 0$. These eigenstates were computed by expansion on a basis set of sine functions. We found 20 states in the potential energy well, their energies are shown on fig. 2. Among them, state # 15 is the most important one for emission, as it is the occupied state with energy closest to the Fermi level.

IV. STATE CURRENT AND CURRENT DENSITY

Fig. 3 shows the emitted current from a single quantum state, the state # 15, which coincides with the Fermi level. We compare the results obtained for the different methods presented in section II. The SFN result corresponds to the analytical potential energy of eq. 10, the three others to the numerical potential energies extracted from VASP outputs using the procedure described in section III B. Results are shown in mA (left scale) and

e^-/fs (right scale). They correspond to a single quantum state filled with one electron (no spin degeneracy). All four curves on fig. 3 show the linear decrease behavior expected from a Fowler-Nordheim (lin-log) type plot. This behavior reflects the tunneling through the potential energy barrier experienced by the electrons emitted from the surface, shown for instance on fig. 2 for 5 GV/m. Saturation corresponds to $D(\epsilon_F) = 1$ in eq. 6. This happens when electrons are transmitted above the potential energy barrier for high enough fields. This occurs above 11.9 GV/m and 7.1 GV/m for the SFN and NFN models respectively. These different thresholds result from differences between the analytical potential energies of eq. 10 and the numerical one. Notice that the transition from the tunneling to the over barrier regime is sudden in the SFN and NFN results, which both correspond to WKB type calculations, and is more gradual for the EQM model, which corresponds to a numerically exact solution of the 1D Schrödinger equation. This represents the only significant difference between the NFN and EQM results, as expected since they both correspond to the same numerical potential energy.

By contrast, the TIP calculation provides results significantly different from the EQM and SFN ones, although it is also performed with the same potential energy. This results from the approximations inherent to this perturbative scheme, as illustrated by fig. 2. The electronic emission is a dynamical process which can be described by the matrix representation of the Hamiltonian (including the external field) in a composite basis including bound states in the metal (dashed and dotted lines on fig. 2) as well as continuum states for the emitted electrons (one of them is the dashed horizontal arrow at the right of fig. 2). The static field induces coupling between all these states, but in our perturbative scheme, only the direct coupling between the initial state - the bound state # 15 - and the final state - the continuum state at exactly the same energy - is considered. This approach neglects higher order processes involving intermediate states, such as those depicted by the arrows of fig. 2. Such second order processes can be computed with a Born expansion of the evolution operator, see for instance ref. 64, p. 23-31. As it is a first order model, the TIP model provides lower current than the EQM and NFN ones, except when saturation is reached in the EQM/NFN models, where the perturbative model is no more adequate. Thus, fig. 3 shows that the simple TIP model provides the right order of magnitude for the current, as expected since it contains the main physical contributors to emission, as long as saturation is not reached. Finally, it should be noticed that the excellent agreement between SFN and

TIP currents on fig. 2 is simply the result of a fortunate cancellation between two differences, namely the use of different potential energies and the use of perturbation theory in the TIP model.

Fig. 4 compares the TIP (lines) and TDP (dots) results for the states # 13, 14 and 15, which correspond to the energies -2.2, -1.1 and 0 eV with respect to the Fermi level. The TIP result for state # 15 is the same as the one of fig. 3. Obviously, the Fermi level is the largest contributor to the emitted current, as the tunneling attenuation is weakest for this state. The agreement between TDP and TIP is excellent, as expected since these are just two numerically different methods to compute the same quantity. However, as the field becomes weaker and current smaller, the TDP method has increasing numerical convergence problems. This can be traced back to the fact that this rate is the Fourier transform given by eq. 15. This integral becomes small when contributions which arise from different time intervals and which can be individually large cancel each other. Small relative errors in several of these contributions turn into a large relative error in the full integral when it is close to zero. The use of the TDP method is therefore limited to large enough fields, albeit simultaneously small enough for the perturbative approximation to remain valid. Fig. 4 shows that the TDP method is valid for currents as low as typically three orders of magnitude below the saturation value. Although this represents a drawback of this method with respect to all the others, it should be pointed out that the TDP method is the only one which can be extended straightforwardly to realistic 3D cases, as no continuum state is required in the computation. Only a simple time propagation of an initially bound state, followed by a Fourier transform, is required. This opens the way for many applications, like the study of the effects of the details of the surface structure like the presence of adsorbates on emission.

Fig. 5 is a usual Fowler-Nordheim plot. The current density is obtained from eq. 12 for the SFN model and from eq. 9 for the NFN, EQM and TIP models, with $I(\epsilon_F)$ as shown on fig. 3, i.e. obtained from eq. 6 for the NFN and EQM models and from eq. 14 for the TIP model. As already discussed on fig. 3, the difference between the SFN result and the others reflects the difference of the potential energies, the difference between NFN and EQM result is due to the approximations inherent to the NFN approach, and TIP results differ from NFN ones because of the approximations of the perturbation theory. The present comparison between perturbative treatments (either time independent or dependent, fig. 4

shows that they are equivalent) and more accurate models, which can be implemented here because the context is one dimensional, shows that perturbative models provide satisfactory results.

Finally, we performed a feasability study of the numerically more challenging TDP-3D method using the three dimensional Kohn-Sham orbitals as initial states in the wavepacket propagation (subsection II E). The current density is now obtained directly from eq. 2 and 3. A critical parameter for convergence is the number of states included in the current summation (eq. 2). We expect the major contribution to come from states near the Fermi level, we retain in the summation the states below Fermi level which are distant in energy by no more than 0.25 eV. Then we did calculations with increasingly denser k-point sampling of the first Brillouin zone. We thus performed 3 batches of calculations including 256, 576 and 900 states in the summation (eq. 2). We found the largest calculation to differ by less than 10% from the smallest one, indicative of acceptable convergence. The results of the largest calculation are shown on fig. 5. The current shows a qualitatively correct behavior as a function of energy, interestingly, the results differs by less than an order of magnitude from the SFN model, although the 3D model describes a physically different situation from the other models which are all one dimensional. We therefore conclude that the TDP-3D method is a promising one to study the effects of the details of the surface structure on emission.

V. CONCLUSION

We described in this paper several models beyond the standard Fowler-Nordheim one to describe electronic emission from first principles. These models all rely on DFT calculations which provide electronic potential energies. Tunneling through the potential energy barriers are described beyond JWKB methods, either by exact or by perturbative quantum mechanical methods. Among these methods, the time dependent perturbative method provides a well balanced trade-off between accuracy and computational cost. These results set future use of perturbative models of realistic cathodes on a safe ground. Studies establishing precise correlations between surface state (defects, corrugation, adsorbates...) and emitted current will be the subject of future work.

VI. ACKNOWLEDGMENTS

We thank Dr. Hubert de Esch, Nadine Halberstadt and Didier Lemoine for useful discussions.

---

* Electronic address: bruno.lepetit@irsamc.ups-tlse.fr

[1] R. H. Fowler and L. Nordheim, Proceedings of the Royal Society of London A: Mathematical, Physical and Engineering Sciences **119**, 173 (1928).

[2] E. L. Murphy and R. H. Good, Physical Review **102**, 1464 (1956).

[3] A. Simonin, J. Achard, K. Achkasov, S. Bechu, C. Baudouin, O. Baulaigue, C. Blondel, J. Boeuf, D. Bresteau, G. Cartry, et al., Nucl. Fusion **55**, 123020 (2015).

[4] A. Simonin, H. d. Esch, L. Doceul, L. Christin, F. Faisse, and F. Villecroze, Fusion Engineering and Design **88**, 1 (2013).

[5] R. S. Hemsworth, A. Tanga, and V. Antoni, Review of Scientific Instruments **79**, 02C109 (2008).

[6] R. Hemsworth, H. Decamps, J. Graceffa, B. Schunke, M. Tanaka, M. Dremel, A. Tanga, H. P. L. de Esch, F. Geli, J. Milnes, et al., Nuclear Fusion **49**, 045006 (2009).

[7] R. V. Latham, *High Voltage Vacuum Insulation: Basic Concepts and Technological Practice* (Elsevier, New-York, 1995).

[8] D. Alpert, D. Lee, E. M. Lyman, and H. E. Tomaschke, Journal of Applied Physics **38**, 880 (1967).

[9] G. Beukema, Physica **61**, 259 (1972).

[10] R. N. Bloomer and B. M. Cox, Vacuum **18**, 379 (1968).

[11] B. Bonin, Vacuum **46**, 907 (1995).

[12] A. Zeitoun-Fakiris and B. Juttner, Journal of Physics D: Applied Physics **21**, 960 (1988).

[13] Y. Yamamoto and T. Miyokawa, Journal of Vacuum Science and Technology B (Microelectronics and Nanometer Structures) **16**, 2871 (1998).

[14] K. Almousa Almaksour, Ph.D. thesis (2014), URL http://www.theses.fr/2014PA112017/document.

[15] K. Almaksour, M. J. Kirkpatrick, P. Dessante, E. Odic, A. Simonin, H. P. L. de Esch, B. Lepetit, D. Alamarguy, F. Bayle, and P. Teste, Phys. Rev. ST Accel. Beams **17**, 103502 (2014).

[16] M. Márquez-Mijares, B. Lepetit, and D. Lemoine, Surface Science **645**, 56 (2016).

[17] M. Márquez-Mijares, B. Lepetit, D. Lemoine, K. Almaksour, M. J. Kirkpatrick, P. Dessante, E. Odic, D. Alamarguy, F. Bayle, P. Teste, et al., J. Vac. Sci. Technol. B **34**, 061208 (2016).

[18] B. Lepetit, D. Lemoine, and M. Márquez-Mijares, J. App. Phys. **120**, 085105 (2016).

[19] R. Gomer and J. K. Hulm, The Journal of Chemical Physics **27**, 1363 (1957).

[20] L. W. Nordheim, Proc. R. Soc. London, Ser. A **121**, 626 (1928).

[21] R. Burgess, H. Kroemer, and J. Houston, Phys. Rev. **90**, 515 (1953).

[22] J. He, P. H. Cutler, and N. M. Miskovsky, App. Phys. Lett. **59**, 1644 (1991).

[23] A. Modinos, Solid-State Electronics **45**, 809 (2001).

[24] R. G. Forbes, App. Phys. Lett. **89**, 113122 (2006).

[25] R. G. Forbes, J. H. B. Deane, A. Fischer, and M. S. Mousa, Jordan Journal of Physics **8**, 125 (2015).

[26] R. G. Forbes and J. H. B. Deane, Proc. R. Soc. London A **467**, 2927 (2011).

[27] S. Parveen, A. Kumara, S. Husain, and M. Husain, Physica B **505**, 1 (2017).

[28] Y. Li, Y. Sun, and J. Yeow, Nanotechnology **26**, 242001 (2015).

[29] Z. B. Li, Ultramicroscopy **159**, 162 (2015).

[30] J. Peng, Z. Li, C. He, G. Chen, W. Wang, S. Deng, N. Xu, X. Zheng, G. Chen, C. J. Edgcombe, et al., Journal of Applied Physics **104**, 014310 (2008).

[31] M. Khazaei, A. A. Farajian, and Y. Kawazoe, Phys. Rev. Lett. **95**, 177602 (2005).

[32] Y. Gohda, Y. Nakamura, K. Watanabe, and S. Watanabe, Phys. Rev. Lett. **85**, 1750 (2000).

[33] Y. Gohda and S. Watanabe, Phys. Rev. Lett. **87**, 177601 (2001).

[34] Y. Gohda and S. Watanabe, Surface Science **516**, 265 (2002).

[35] Y. Gohda, Y. Nakamura, K. Watanabe, and S. Watanabe, Materials Science and Engineering A **327**, 1 (2002).

[36] Y. Gohda and S. Watanabe, J. Phys.: Condens. Matter **16**, 4685 (2004).

[37] S. F. Huang, T. Leung, B. Li, and C. Chan, Phys. Rev. B **72**, 035449 (2005).

[38] A. Mayer, N. M. Miskovsky, P. H. Cutler, and P. Lambin, Phys. Rev. B **68**, 235401 (2003).

[39] Z. Li, N. Xu, and H. J. Kreuzer, Phys. Rev. B **85**, 115427 (2012).

[40] P. Yaghoobi, K. Walus, and A. Nojeh, Phys. Rev. B **80**, 115422 (2009).

[41] S. Han, M. H. Lee, and J. Ihm, Phys. Rev. B **65** (2002).

[42] Y.-W. Son, S. Oh, J. Ihm, and S. Han, Nanotechnology **16**, 125 (2005).

[43] C. Choong-Ki Lee, B. Lee, and S. Ihm, J. Han, Nanotechnology **18**, 475706 (2007).

[44] C. Kittel, *Introduction to solid state physics* (Wiley, 1996), 7th ed.

[45] D. S. Sholl and J. A. Steckel, *Density functional theory: a practical introduction* (Wiley, Hoboken, N.J, 2009).

[46] R. G. Forbes, Surf. Interface Anal. **36**, 395 (2004).

[47] L. D. Landau and E. M. Lifshitz, *Quantum mechanics. Non relativistic theory. Course of theoretical physics. Vol. 3* (Pergamon Press, 1965), 2nd ed.

[48] A. Mayer, Journal of Vacuum Science and Technology B, Nanotechnology and Microelectronics: Materials, Processing, Measurement, and Phenomena **29**, 021803 (2011).

[49] A. Messiah, *Quantum mechanics. Vol. 2* (North Holland, 1961).

[50] P. Villareal, S. Miret-Artés, O. Roncero, D. Delgado-Barrio, J. A. Beswick, N. Halberstadt, and R. D. Coalson, J. Chem. Phys. **94**, 4230 (1991).

[51] G. Kresse and J. Hafner, Physical Review B **47**, 558 (1993).

[52] G. Kresse and J. Hafner, Physical Review B **49**, 14251 (1994).

[53] G. Kresse and J. Furthmüller, Computational Materials Science **6**, 15 (1996).

[54] G. Kresse and J. Furthmüller, Physical Review B **54**, 11169 (1996).

[55] P. E. Blöchl, Physical Review B **50**, 17953 (1994).

[56] G. Kresse and D. Joubert, Physical Review B **59**, 1758 (1999).

[57] J. P. Perdew, K. Burke, and M. Ernzerhof, Physical Review Letters **77**, 3865 (1996).

[58] J. P. Perdew, K. Burke, and M. Ernzerhof, Physical Review Letters **78**, 1396 (1997).

[59] Y. Zhang and W. Yang, Physical Review Letters **80**, 890 (1998).

[60] M. Methfessel and A. Paxton, Physical Review B **40**, 3616 (1989).

[61] R. M. Feenstra and M. Widom, waveTrans : real-space wavefunctions from VASP Wavecar file, URL `http://www.andrew.cmu.edu/user/feenstra/wavetrans/`.

[62] R. G. Forbes, Ultramicroscopy **73**, 31 (1998).

[63] R. G. Forbes, Ultramicroscopy **79**, 25 (1999).

[64] C. Cohen-Tannoudji, J. Dupont-Roc, and G. Grynberg, *Atom-photon interactions. Basic processes and applications* (Wiley, 1992).

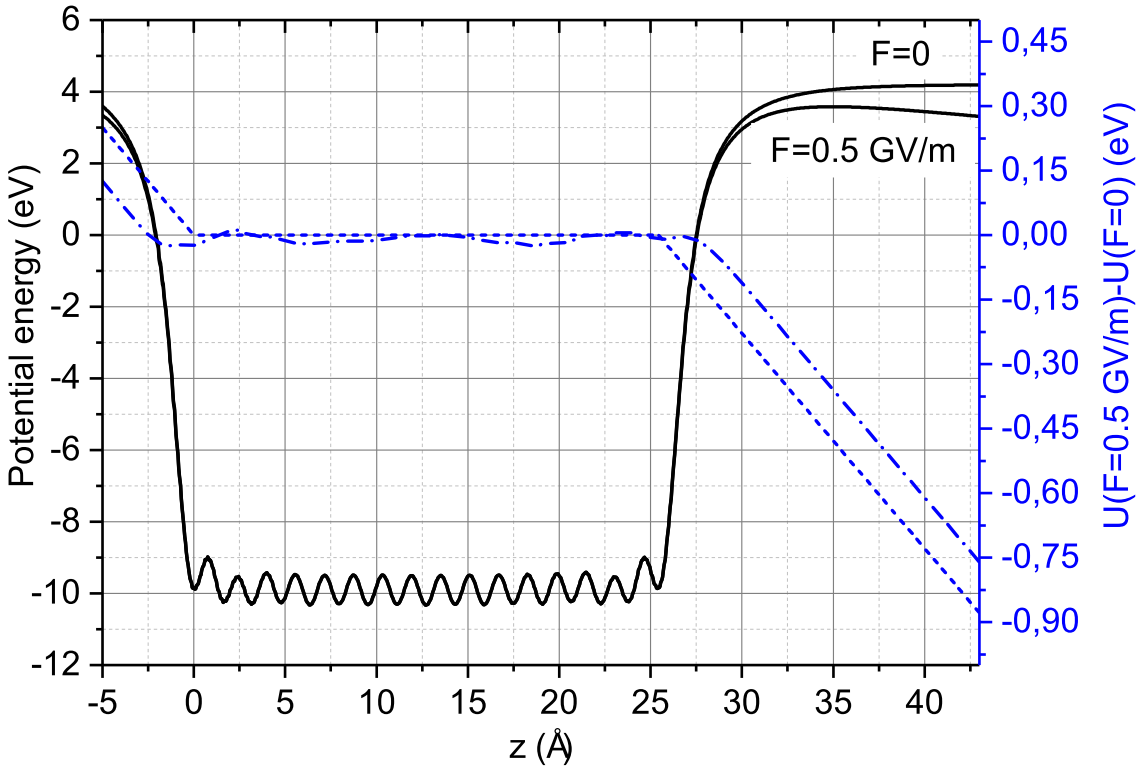

FIG. 1: Full lines (left scale) : total (Hartree+exchange-correlation) potential energy for external fields $F = 0.5$ GV/m and $F = 0$. The potential energies are shown along the z line perpendicular to the slab and defined by : $x = a/2$, $y = 0$. There is no tungsten atom on this line so that the potential energy curves have only limited undulations (inside the slab) : the 17 minima are located at the intersections of this line with the perpendicular atomic planes. The zero energy is the Fermi level. The work function is 4.2 eV. Dashed-dotted line (right scale) : difference $U(F = 0.5 \text{ GV/m}) - U(0)$ of the Hartree potential energies obtained from VASP simulations for $F = 0.5$ GV/m and $F = 0$ external fields. Dashed line (right scale) : simple linear potential energy curve $-eF(z - z_s)$ for $F = 0.5$ GV/m. z_s refers to the last atomic plane position before vacuum. The difference $U(F = 0.5 \text{ GV/m}) - U(0)$ follows closely this simple linear dependence, but shifted away from the slab by nearly 2 $\AA$, which corresponds to the "repulsion distance" described in refs. 18,62,63.

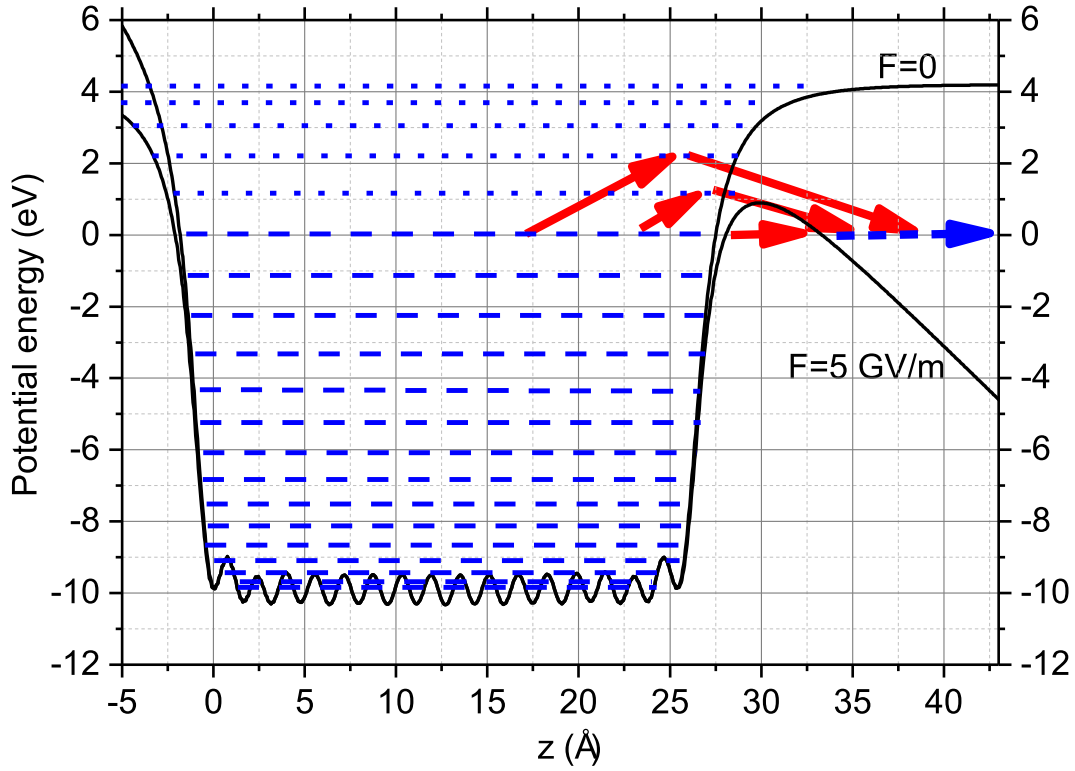

FIG. 2: Full lines : 1D total (Hartree+exchange-correlation) potential energy along the line $x = a/2$, $y = 0$, for the two external field values 0 and 5 GV/m. The zero energy is the Fermi level. Dashed lines : bound state energies in the $F = 0$, 1D potential energy curve, up to the Fermi level. The zero energy continuum state is also symbolized by a dashed arrow. Dotted lines : bound states in the $F = 0$, 1D potential energy curve, above the Fermi level. Arrows indicate possible dynamical transition processes between the Fermi level and the zero energy continuum state, either direct tunneling through the barrier or virtual transitions to intermediate excited states.

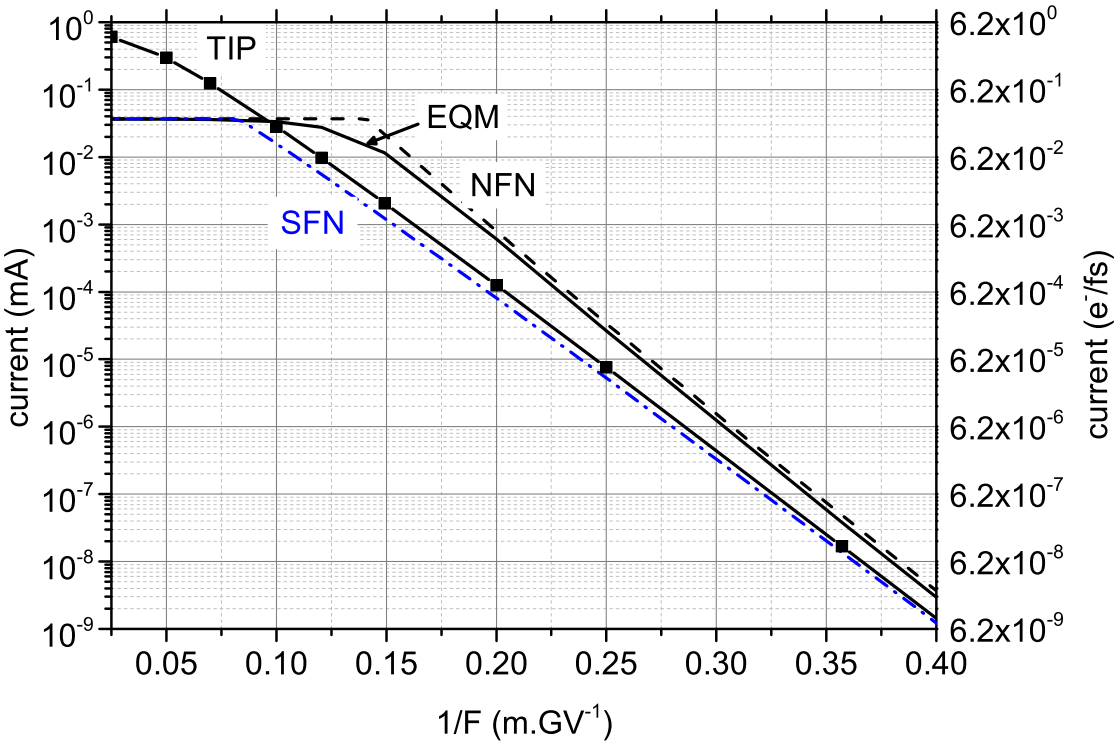

FIG. 3: State currents from state # 15 at the Fermi energy : comparison between TIP (full line+squares), EQM (full line), NFN (dashed line) and SFN (dashed-dotted line) results. Currents are given in mA (left scale) and in number of electrons per femtosecond (e^-/fs, right scale). The SFN result is obtained from eq. 6 and eq. 11, it corresponds to the potential energy given by eq. 10. The EQM and NFN results are obtained from eq. 6 and corresponding tunneling probabilities (see subsection II C) for the one-dimensional numerical potential energy obtained from VASP calculations (see subsection III B). The TIP result is obtained from eq. 14, also for the 1D potential energy extracted from VASP results.

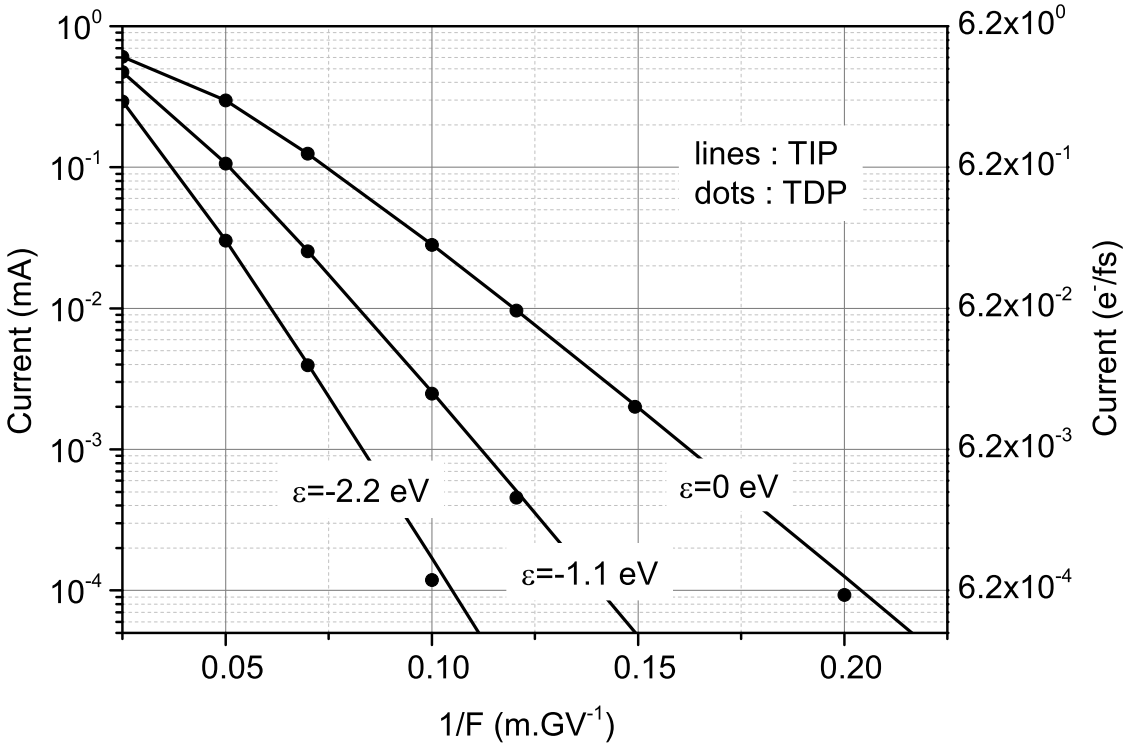

FIG. 4: State currents for the states # 13, 14 and 15, which correspond to the energies ϵ = -2.2, -1.1 and 0 eV with respect to the Fermi level. Comparison between TIP results (full line) and TDP ones (dots). Currents are given in mA (left) and in number of electrons per femtosecond (e^-/fs, right). The TIP result for state # 15 is the same as the one of fig. 3.

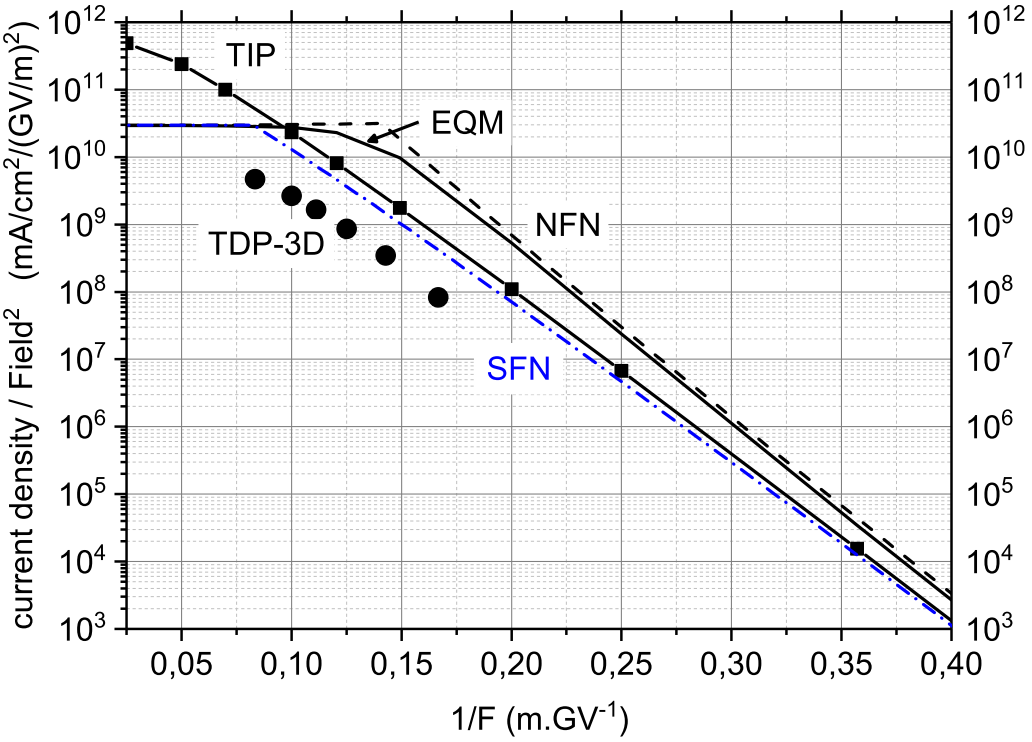

FIG. 5: Fowler-Nordheim plot : total emitted current density divided by the field squared vs inverse field : TIP (full line+squares), EQM (full line), NFN (dashed line) and SFN (dashed-dotted line) results. Dark circles are the results of the time dependent perturbation method calculation on the full 3 dimensional structure (TDP-3D).